Assessment of Electron-Proton Correlation Functionals for Vibrational Spectra of Shared-Proton Systems by Constrained Nuclear-Electronic Orbital Density Functional Theory

Yuzhuo Yang,[1] Yuzhe Zhang,[2] Yang Yang,[2, a)] and Xi Xu[1, b)]

[1)] *Center for Advanced Materials Research, Beijing Normal University, Zhuhai 519087, China*

[2)] *Theoretical Chemistry Institute and Department of Chemistry, University of Wisconsin-Madison, Madison, Wisconsin 53706, United States*

(Dated: 19 November 2024)

Proton transfer plays a crucial role in various chemical and biological processes. A major theoretical challenge in simulating proton transfer arises from the quantum nature of the proton. The constrained nuclear-electronic orbital (CNEO) framework was recently developed to efficiently and accurately account for nuclear quantum effects, particularly quantum nuclear delocalization effects, in quantum chemistry calculations and molecular dynamics simulations. In this paper, we systematically investigate challenging proton transfer modes in a series of shared-proton systems using CNEO density functional theory (CNEO-DFT), focusing on evaluating existing electron-proton correlation functionals. Our results show that CNEO-DFT accurately describes proton transfer vibrational modes and significantly outperforms conventional DFT. The inclusion of the epc17-2 electron-proton correlation functional in CNEO-DFT produces similar performance to that without electron-proton correlations, while the epc17-1 functional yields less accurate results, comparable to conventional DFT. These findings hold true for both asymmetrical and symmetrical shared-proton systems. Therefore, until a more accurate electron-proton correlation functional is developed, we currently recommend performing vibrational spectrum calculations using CNEO-DFT without electron-proton correlation functionals.

[a)]Electronic mail: yyang222@wisc.edu

[b)]Electronic mail: xuxi@bnu.edu.cn

I. INTRODUCTION

Proton transfer is a fundamental process in many chemical and biological systems. A well-known example is the proton transfer through the hydrogen bond network in liquid water, which accounts for the anomalously high mobility of protons in aqueous systems.[1] Shared-proton systems, in which a proton is shared between two closed-shell molecular fragments, are prototypical models to further understand proton transfer in condensed phases. For example, a proton equally shared by two water molecules, known as the Zundel ion, is considered to be one of the fundamental structural motifs in the proton transfer process in water and has been extensively studied for many years.[2–10]

A significant challenge in the theoretical treatment of proton transfer comes from the quantum nature of protons.[11–13] In conventional quantum chemistry methods, nuclei are treated as classical particles. However, because of the low mass of protons, their nuclear quantum effects (NQEs) can not be ignored in many cases. For instance, proton delocalization and proton tunneling substantially influence structures and dynamics of water.[12,14] In enzymes, strong hydrogen bonds and associated NQEs play a crucial role in lowering activation barriers and facilitating rapid and efficient chemical transformations.[15]

Many theoretical methods have been developed to incorporate NQEs, mainly including quantum dynamics methods,[16,17] path-integral approaches,[18,19] and multicomponent quantum chemistry methods.[20–22] Recently, constrained nuclear-electronic orbital density functional theory[23] (CNEO-DFT) was developed within the multicomponent quantum chemistry framework and has been shown to efficiently and accurately describe vibrational modes involving hydrogen atoms.[24] Unlike other multicomponent quantum chemistry methods, the CNEO framework is based on the key physical fact that, while quantum nuclei have density distributions delocalized in space similar to electrons, yet they are much more localized than those of electrons. Therefore, nuclear expectation positions can be used to represent the classical positions for nuclei. As such, the treatment of nuclei in CNEO is both quantum and classical, which is achieved by introducing constraints on nuclear expectation positions in the Lagrangian of multicomponent systems. The total energy minimized under these constraints leads to the CNEO energy surfaces.[23]

The CNEO energy surface is analogous to the Born-Oppenheimer potential energy surface, but is an effective energy surface with NQEs incorporated. Both analytic gradients and

analytic Hessian of the CNEO enengy surface have been developed,[24,25] making it possible to incorporate NQEs, especially quantum nuclear delocalization effects, into structural optimization, transition state search, and molecular dynamics simulations. In particular, the combination of CNEO with molecular dynamics[26,27] (CNEO-MD) has significantly expanded its range of applications. Tests on a series of molecular systems demonstrated that CNEO-MD provides an accurate description of molecular vibrational frequencies, particularly for those vibrational modes involving hydrogen atoms.[26,28–33] Furthermore, CNEO shows great promise for hydrogen atom transfer reactions, which gives accurate rate constants but with computational costs comparable to conventional DFT-based transition state theory.[34]

In previous studies on molecular vibrations with CNEO-DFT, interactions between electrons and protons were limited to mean-field Coulomb interactions, while electron-proton correlations were neglected. Therefore, the impact of electron-proton correlations in CNEO-DFT on vibrational spectra awaits systematic studies, especially since it was well known that electron-proton correlations can be crucial in the accurate description of proton densities and protonic affinities in conventional NEO-DFT.[35–38] In this paper, we address this question by systematically investigating a series of shared-proton systems. Specially, we investigate 16 [A·H^+·B] type binary complexes (Fig. 1) and focus on their most challenging proton transfer modes (PTMs). Here A and B include H_2O, NH_3, CO_2, Ar, MeOH (Me = CH_3), EtOH (Et = CH_2CH_3), Me_2O and Et_2O.

This paper is organized as follows. A brief review of the basic concepts and theoretical formulation of CNEO-DFT will be presented in Sec. II to ensure the paper is self-contained. Next, computational details for both conventional DFT and CNEO-DFT will be provided in Sec. III. The results and discussions on the vibrational frequencies and intensities of these shared-proton systems will be presented in Sec. IV. Finally, concluding remarks and potential future directions are given in Sec. V.

II. THEORETICAL METHODS

In this section, we briefly review the theoretical framework of CNEO-DFT. For simplicity, we only treat protons and electrons quantum mechanically. A detailed formulation of CNEO-DFT, including a full-quantum treatment on all nuclei, can be found in previous work.[23,25]

According to the generalization of the Hohenberg-Kohn theorem to a quantum multi-

component system of electrons and nuclei,[39] the ground-state energy of the multicomponent system is a functional of both the electron density ρ^e and the proton density ρ^p,

$$E_{\text{g.s.}} = E[\rho^e, \rho^p]. \tag{1}$$

Within the multicomponent Kohn-Sham formalism, the energy can be further expressed as[35]

$$\begin{aligned} E[\rho^e, \rho^p] = (T_s[\rho^e] + T_s[\rho^p]) + (J^{ee}[\rho^e] + J^{pp}[\rho^p] + J^{ep}[\rho^e, \rho^p]) + \\ + (E^e_{\text{xc}}[\rho^e] + E^p_{\text{xc}}[\rho^p]) + (E_{\text{epc}}[\rho^e, \rho^p]) + (E^e_{\text{ext}}[\rho^e] + E^p_{\text{ext}}[\rho^p]), \end{aligned} \tag{2}$$

where the quantities in each parenthesis represent the non-interacting kinetic energy of electrons and protons, the mean-field Coulomb interaction energy between electrons and protons, the exchange-correlation energy of electrons and protons, the electron-proton correlation energy, and the external potential energy, respectively. Electron and proton densities can be obtained using the corresponding orbitals,

$$\rho^e = \sum_i^{N^e} |\phi^e_i|^2, \tag{3}$$

$$\rho^p = \sum_I^{N^p} |\phi^p_I|^2, \tag{4}$$

in which N^e is the number of electrons and N^p is the number of protons.

In practical chemical systems, protons are relatively localized compared to electrons, and their spatial overlap is negligible. Therefore, each proton can be treated as a distinguishable particle with a localized orbital. The proton-proton exchange and correlation energies are negligible and can be approximated using the diagonal Hartree-Fock exchange terms to eliminate self-interaction errors. Based on the localized nature of protons in molecular systems, we impose a constraint on the expectation position for each proton in the CNEO framework,[23]

$$\langle \phi^p_I | \mathbf{r} | \phi^p_I \rangle = \mathbf{R}_I. \tag{5}$$

With this constraint and the normalization requirement for orbitals, the Lagrangian for the multicomponent system can be written as

$$L = E + \sum_I^{N^p} \mathbf{f}_I \cdot (\langle \phi^p_I | \mathbf{r} | \phi^p_I \rangle - \mathbf{R}_I) - \sum_i^{N^e} \epsilon^e_i (\langle \phi^e_i | \phi^e_i \rangle - 1) - \sum_I^{N^p} \epsilon^n_I (\langle \phi^p_I | \phi^p_I \rangle - 1), \tag{6}$$

where $\mathbf{f}_I$ is the Lagrange multiplier associated with the constraints on expectation positions for the I-th proton. Making the Lagrangian stationary with respect to orbital variations leads to the Kohn-Sham-like equations for electrons,

$$(-\frac{1}{2}\nabla^2 + v_J^{ee} + v_J^{pe} + v_{\rm xc}^e + v_{\rm epc}^e + v_{\rm ext}^e)\phi_i^e = \epsilon_i^e \phi_i^e, \tag{7}$$

and for protons,

$$(-\frac{1}{2M_p}\nabla^2 + v_J^{pp} + v_J^{ep} + v_{\rm xc}^n + v_{\rm epc}^p + v_{\rm ext}^p + \mathbf{f}_I \cdot \mathbf{r})\phi_I^p = \epsilon_I^p \phi_I^p, \tag{8}$$

where each term in the Fock-like operator on the left side of the equations is obtained by taking the functional derivative of the corresponding energy term in Eq. 2 with respect to either the electron density or the proton density. In the Fock-like operator for the nuclear equations, an extra term $\mathbf{f}_I \cdot \mathbf{r}$ shows up due to the constraints on the nuclear expectation positions. The equations 7 and 8 are coupled and can be solved iteratively together with the Lagrangian multipliers $\{\mathbf{f}_I\}$.[25]

The epc17 family of electron-proton correlation functions was developed analogously to the Lee-Yang-Parr (LYP) electron correlation functional,[40] and more details can be found in Ref. 35. Based on a local density approximation, the electron-proton correlation functional takes the form

$$E_{\rm epc}[\rho^e, \rho^p] = -\int {\rm d}\mathbf{r} \frac{\rho^e(\mathbf{r})\rho^p(\mathbf{r})}{a - b[\rho^e(\mathbf{r})]^{1/2}[\rho^p(\mathbf{r})]^{1/2} + c\rho^e(\mathbf{r})\rho^p(\mathbf{r})}, \tag{9}$$

where a, b and c are parameters for the functional. The epc17-1 functional[35] was optimized to reproduce proton densities with parameters $a = 2.35$, $b = 2.4$ and $c = 3.2$, while the epc17-2 functional[36] was optimized to reproduce absolute zero-point energies with parameters $a = 2.35$, $b = 2.4$ and $c = 6.6$. Note that the only difference between these the two functionals is the value of the parameter c. The electron-proton correlation potential for electrons and protons can be obtained by taking the functional derivative of $E_{\rm epc}$ with respect to the electron density or the proton density, respectively.

$$v_{\rm epc}^e(\mathbf{r}) = \frac{\delta E_{\rm epc}}{\delta \rho^e(\mathbf{r})} = -\frac{a\rho^p(\mathbf{r}) - \frac{b}{2}[\rho^e(\mathbf{r})]^{1/2}[\rho^p(\mathbf{r})]^{3/2}}{\left(a - b[\rho^e(\mathbf{r})]^{1/2}[\rho^p(\mathbf{r})]^{1/2} + c\rho^e(\mathbf{r})\rho^p(\mathbf{r})\right)^2} \tag{10}$$

$$v_{\rm epc}^p(\mathbf{r}) = \frac{\delta E_{\rm epc}}{\delta \rho^p(\mathbf{r})} = -\frac{a\rho^e(\mathbf{r}) - \frac{b}{2}[\rho^e(\mathbf{r})]^{3/2}[\rho^p(\mathbf{r})]^{1/2}}{\left(a - b[\rho^e(\mathbf{r})]^{1/2}[\rho^p(\mathbf{r})]^{1/2} + c\rho^e(\mathbf{r})\rho^p(\mathbf{r})\right)^2} \tag{11}$$

III. COMPUTATIONAL DETAILS

We implemented CNEO-DFT as well as its analytic gradients with the epc17-1 and epc17-2 functionals in a locally modified version (`https://github.com/theorychemyang/pyscf`) of the PySCF[41,42] package. All *ab initio* DFT and CNEO-DFT calculations were carried out with the modified PySCF package. Geometry optimization was performed through an interface between the PySCF package and the Atomic Simulation Environment (ASE) package.[43] For each molecule, harmonic vibrational analysis was carried out based on the optimized geometric structure.

The electronic exchange-correlation functional can have a considerable influence on molecular vibrational frequencies. In previous work,[28] several exchange-correlation functionals, including B3LYP,[40,44] PBE0,[45] and ωB97X,[46] has been tested against the results from the gold standard CCSD(T) method.[47] For the PTMs in $H_5O_2^+$ and $H_3O_2^-$, the ωB97X functional, when combined with the aug-cc-pVDZ basis set,[48] was found to provide the best agreement with CCSD(T) results with a large basis set.[28] Because of the large computational cost of CCSD(T), it is impractical to benchmark larger shared proton systems; therefore, in this work, we continue to use the ωB97X functional as the electronic exchange-correlation functional and the aug-cc-pVDZ basis as the electronic basis set for all calculations.

In [A·H$^+$·B] clusters, the dispersion interactions between the two tethered molecular fragments have not been extensively studied. To assess the necessity for dispersion corrections,[49] we took the $H_5O_2^+$ ion as an example and investigated the dependence of vibrational frequencies on dispersion interaction corrections. The dispersion interaction corrections are taken into account with the Becke-Johnson D3 correction scheme[50,51] and the results are presented in Table S1. We find that for the frequency of the PTM in $H_5O_2^+$, dispersion interaction corrections can lead to a blue shift of about 100 cm^{-1}. This shift is not negligible, however, it also causes the frequency to diverge from the reference value of CCSD(T), which may indicate that the original ωB97X with the aug-cc-pVDZ basis set benefits from a delicate error cancellation, and adding dispersion corrections breaks the balance and introduces larger errors to the electronic parts. Furthermore, as noted by Ref. 52, the inclusion of dispersion with most functionals could yield large errors for hydrogen bonded systems. Consequently, we did not incorporate dispersion interaction corrections in our calculations.

For CNEO-DFT calculations, the same electronic exchange-correlation functional and

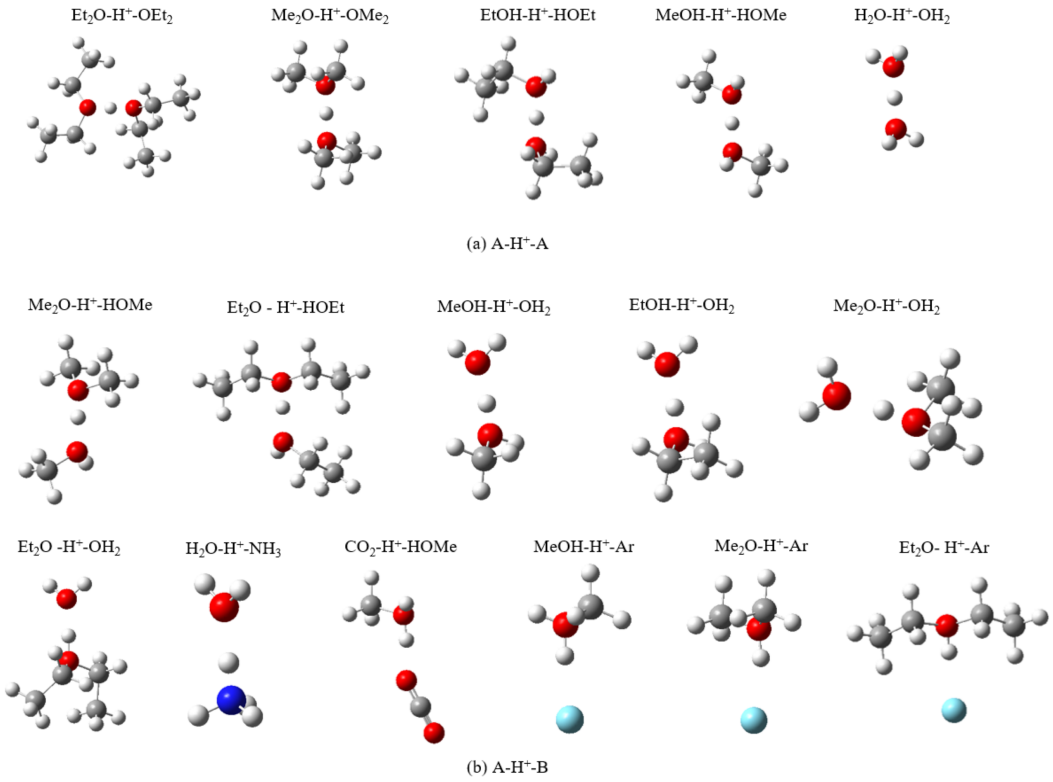

FIG. 1: Shared-proton complexes investigated in this work

electronic basis set are adopted for comparison. We only treated hydrogen nuclei quantum mechanically because heavier nuclei typically have smaller NQE than hydrogens. However, we note that a full quantum treatment is also possible with the CNEO framework.[25] All hydrogens in the shared proton systems were treated quantum mechanically in our calculations, with the exception of the $Et_2O-H^+-OEt_2$ molecule, which contains 20 hydrogen atoms. Since we are mainly interested in the proton transfer mode, only the shared proton of this molecule was treated quantum mechanically, while the other protons were treated classically. The classic treatment on these non-PTM hydrogens is expected to have a relatively minor impact on the frequency of the PTM. The PB4D basis[53] is used for quantum protons, which demonstrated accuracy and efficiency for vibrational analyses in previous studies.[26,28,30,33] To explore the impacts of electron-proton correlations on molecular vibrations, particularly on proton transfer modes, the CNEO calculations were performed with the inclusion of the epc17-1 functional or the epc17-2 functional, and the results were compared with those at the no-epc level, which neglects all electron-proton correlation.

TABLE I: Harmonic vibrational frequencies (in cm^{-1}) of proton transfer modes in [A·H^+·B] type clusters by DFT and CNEO-DFT.

Molecule	Experiment[a]	DFT	CNEO/no-epc	CNEO/epc 17-1	CNEO/epc17-2
Me_2O-H^+-HOMe	1595	2273.8	1752.6	2265.3	1805.5
Et_2O-H^+-HOEt	1638	2514.8	1990.6	2435.0	2041.1
$MeOH-H^+-OH_2$	1828	2361.9	1933.5	2386.4	1977.3
$EtOH-H^+-OH_2$	1964	2534.1	2088.2	2554.0	2142.4
$Me_2O-H^+-OH_2$	2094	2751.5	2311.9	2746.5	2358.6
$Et_2O-H^+-OH_2$	2310	2876.2	2481.5	2856.3	2542.7
$H_2O-H^+-NH_3$	2649	2899.5	2581.2	2892.1	2613.8
CO_2-H^+-HOMe	3064	3279.6	2978.8	3295.8	3037.4
$MeOH-H^+-Ar$	3330	3518.9	3283.1	3520.2	3323.3
Me_2O-H^+-Ar	3403	3619.6	3382.8	3598.9	3408.8
Et_2O-H^+-Ar	3431	3650.7	3423.3	3624.1	3445.7
MAE	-	452	123	443	139

a. From Ref. 54.

IV. RESULTS AND DISCUSSION

A. [A·H^+·B] type clusters

We optimized the molecular geometry and performed harmonic analysis for 11 [A·H^+·B] type clusters using DFT and CNEO-DFT. The X-H bond lengths in the optimized structures are listed in Table S2, where X stands for the heavy atom which is closer to the shared proton. The harmonic vibrational frequencies of the PTMs in these clusters are presented in Table I, along with experimental references.[54] DFT harmonic calculations consistently overestimate the vibrational frequencies of these modes, with a mean absolute error (MAE) of 452 cm^{-1}. In contrast, the MAE significantly reduces to 123 cm^{-1} when using CNEO-DFT without electron-proton correlations. This finding is consistent with the previous results,[24] showing that CNEO-DFT, even with a purely harmonic treatment, can accurately describe hydrogen-related vibrations as a result of the quantum delocalized proton picture. Incorporating

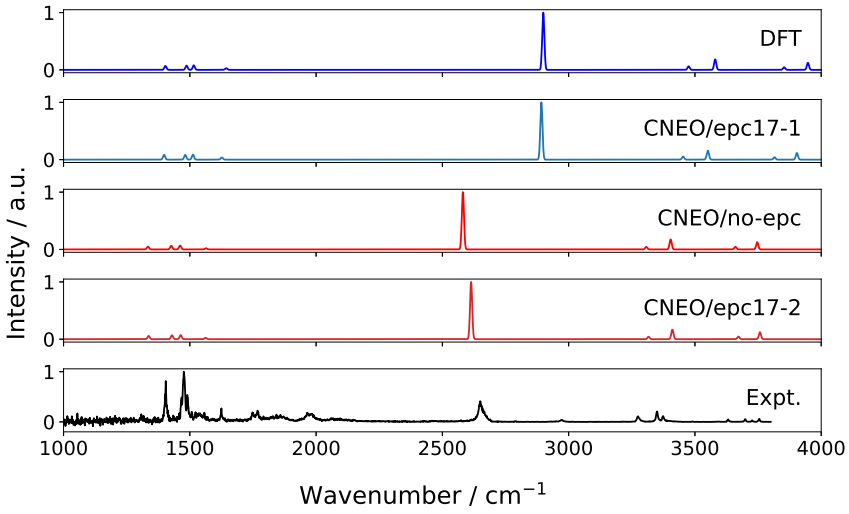

FIG. 2: Harmonic IR spectra of $H_2O-H^+-NH_3$ from DFT and CNEO-DFT with different levels of electron-proton correlations. Experimental IR spectrum is taken from Ref. 54

electron-proton correlations through the epc17-2 functional does not qualitatively alter the results, with the MAE slightly increased to 139 cm^{-1}. However, applying electron-proton correlations via the epc17-1 functional leads to a significant overestimation of vibrational frequencies, which raises the MAE to 443 cm^{-1}. Interestingly, the performance of CNEO-DFT with the epc17-1 functional is very similar to that of conventional DFT, despite the fact that the epc17-1 functional produces the most delocalized nuclear densities.[35]

In Fig. 2, we use the $H_2O-H^+-NH_3$ cluster to demonstrate the performance of DFT and CNEO-DFT on the IR spectrum of [A·H$^+$·B] type clusters. The experimental IR spectrum shows a moderate-intensity PTM at 2649 cm^{-1}. Both CNEO-DFT without electron-proton correlations and CNEO-DFT with the epc17-2 functional accurately capture the frequency of this mode, while DFT and CNEO-DFT with the epc17-1 functional overestimate it. Regarding intensity, all DFT and CNEO-DFT methods predict the PTM to be the most intense peak, which contrasts with the moderate intensity observed in the experimental spectrum. The reason for this discrepancy in intensity remains unclear and requires further investigation. For the free N-H and O-H stretches appearing above 3300 cm^{-1}, we again find that both CNEO-DFT methods (no-epc and epc17-2) yield the most accurate results. In contrast, the performance of DFT and CNEO-DFT with the epc17-1 functional is similar, with both methods overestimating the vibrational frequencies. Therefore, the good performance of CNEO-DFT with no-epc or epc17-2 is consistent for both bonded X-H vibrations and

TABLE II: Harmonic frequencies (in cm^{-1}) of proton transfer modes in [A·H^+·A] type clusters by DFT and CNEO-DFT.

Molecule	Experiment[a]	DFT	CNEO/no-epc	CNEO/epc17-1	CNEO/epc17-2
$Et_2O-H^+-OEt_2$	842	908.1	926.2	898.3	914.7
$Me_2O-H^+-OMe_2$	952	660.2	995.7	683.3	988.0
EtOH$-H^+-$HOEt	840	892.3	850.9	874.7	837.7
MeOH$-H^+-$HOMe	887	630.3	902.6	636.0	892.5
$H_2O-H^+-OH_2$	1002	816.6	1126.3	785.0	1096.6
MAE	-	170	56	166	42

a. From Ref. 54.

free X-H vibrations.

B. [A·H^+·A] type clusters

We investigate 5 [A·H^+·A] type clusters in this work. As with the [A·H^+·B] type clusters, we optimized the molecular geometries and the predicted O-H distances for the optimized structures are presented in Table S2. Both conventional DFT and CNEO-DFT predict that the shared proton is either equally or nearly equally shared between the two molecular fragments. The harmonic vibrational frequencies are listed in Table II. We note that in [A·H^+·A] type clusters, multiple peaks may all exhibit proton transfer characteristics and form a band of PTMs. The experimental frequencies are based on the centroids of these bands.[54] For comparison with experimental values, the calculated frequencies are intensity-weighted within the range of 600 to 1100 cm^{-1}. Similar to the [A·H^+·B] type clusters, CNEO-DFT, whether without electron-proton correlations or with the epc17-2 functional, yields accurate frequencies with MAEs around 50 cm^{-1}, although in this case, the epc17-2 functional offers slightly more accurate results. In contrast, DFT and CNEO-DFT with the epc17-1 functional are less accurate with MAEs exceeding 150 cm^{-1}. The largest error occur in the MeOH$-H^+-$HOMe and $Me_2O-H^+-OMe_2$ systems, where both DFT and CNEO-DFT/epc17-1 significantly underestimate the PTM frequencies by more than 200 cm^{-1}.

The calculated harmonic IR spectra of MeOH$-H^+-$HOMe, EtOH$-H^+-$HOEt, $Me_2O-H^+-OMe_2$

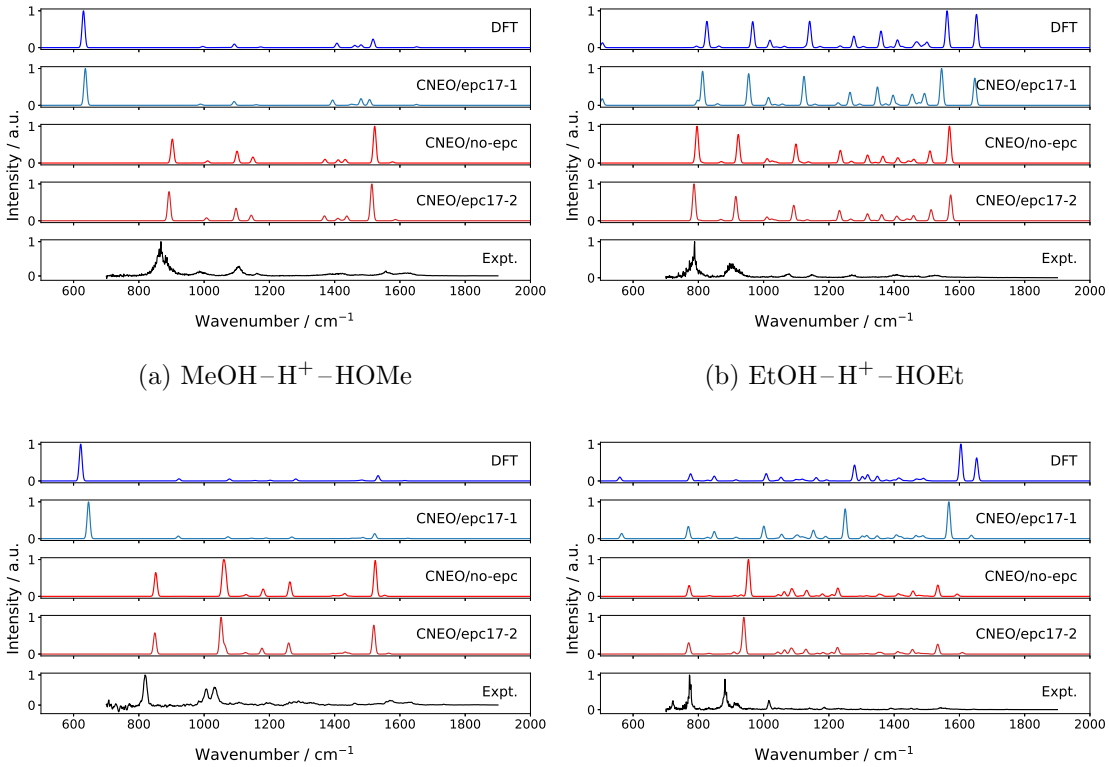

(a) MeOH$-$H$^+-$HOMe

(b) EtOH$-$H$^+-$HOEt

(c) Me$_2$O$-$H$^+-$OMe$_2$

(d) Et$_2$O$-$H$^+-$OEt$_2$

FIG. 3: Harmonic IR spectra by DFT and CNEO-DFT with different levels of electron-proton correlations. Experimental IR spectra are from Ref. 54.

and Et$_2$O$-$H$^+-$OEt$_2$ by DFT and CNEO-DFT are presented and compared with experimental spectra in Fig. 3. In general, conventional DFT faces great challenges with large errors both in peak positions and peak intensities, particularly for those PTMs. For the two challenging MeOH$-$H$^+-$HOMe and Me$_2$O$-$H$^+-$OMe$_2$ systems, DFT predicts the PTMs to have the highest intensities, but the intensities of other peaks are too low compared with experimental results. Normal mode analysis shows that in harmonic DFT calculations, the proton transfer motion does not couple with other vibrational modes and does not lend intensities to the remaining modes. For EtOH$-$H$^+-$HOEt and Et$_2$O$-$H$^+-$OEt$_2$, the intensities of the PTMs are much lower, and DFT shows strongest peaks around 1600 cm^{-1}, which primarily originate from the O-H-O bending. The calculated IR spectra from CNEO-DFT with the epc17-1 functional are overall similar to those from DFT, although there are some subtle differences in peak positions and intensities.

In contrast, the peak positions and intensities from both CNEO-DFT without electron-

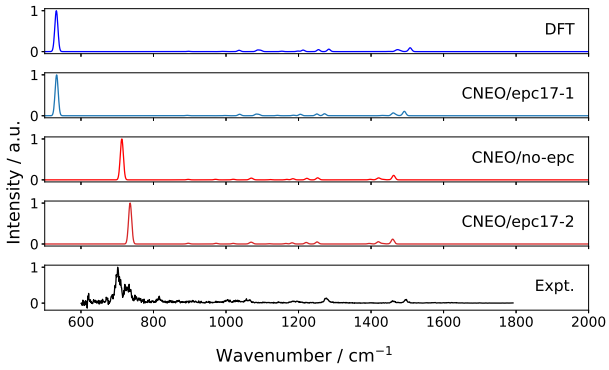

FIG. 4: Harmonic IR spectra of $Me_2O-D^+-OMe_2$ by DFT and CNEO-DFT. Experimental IR spectra are from Ref. 54.

proton correlations and CNEO-DFT with the epc17-2 functional align much more closely with the experimental IR spectra. Normal mode analysis shows that many peaks in the range of 800 to 1100 cm^{-1} have proton transfer characters. For example, in Fig. S1, we show that in $MeOH-H^+-HOMe$, proton transfer is involved in multiple normal modes. The frequencies and relative intensities of the these modes generally agrees well with experimental results. However, a major discrepancy is that in all four systems, the peak slightly below 1600 cm^{-1} is too intense compared with experimental results. The reason for this discrepancy is unclear, as these peaks are also mainly associated with proton transfer, and no peaks are dominated by O-H-O bending.

To explore the performance of epc in heavier isotopes of hydrogen and the possible impact of isotope substitution on PTMs, we used the $Me_2O-D^+-OMe_2$ complex as an example and calculated its IR spectrum using DFT and CNEO-DFT. The calculated and experimental IR spectra are shown in Fig. 4. The results are similar to those in Fig. 3(c), except the peaks related to the hydrogen motion are overall redshifted. CNEO-DFT with no-epc and epc17-2 again exhibit the best agreement with the experiments. Interestingly, in the deuterated case, the intensities of those peaks between 1000 cm^{-1} and 1600 cm^{-1} are no longer overestimated as in the undeuterated case. According to experimental results, the peak of the PTM has a red shift of about 150 cm^{-1} upon deuterium substitution. This effect is accurately captured by CNEO-DFT with both no-epc and epc17-2. However, DFT and CNEO-DFT with the epc17-1 functional predict the red shift to be less than 100 cm^{-1}, and the frequency of the PTM is greatly underestimated. Therefore, the performance of CNEO-DFT with different electron-nuclear correlation functionals for deuterated species is consistent with previous

findings for the corresponding undeuterated species.

C. Proton densities versus vibrational frequencies

It has been known in the multicomponent quantum chemistry community that, without electron-proton correlations, calculated proton densities tend to be over-localized. The inclusion of electron-proton correlations, particularly with functionals such as epc17-1, can lead to more delocalized proton densities, which better align with grid-based methods.[35] The delocalization of proton densities received considerable attention because it was used to obtain proton vibrational frequencies before the development of NEO time-dependent density functional theory[55,56] (NEO-TDDFT) and the invention of the CNEO framework.[23] As such, many electron-proton correlation functionals, including the epc17, epc18,[37] and epc19[38] families were developed to yield more delocalized proton densities compared to calculations without electron-proton correlations. Calculations at the no-epc level produce the most localized proton densities, while the inclusion of the epc17-1 functional generates the most delocalized densities, with the epc17-2 functional falling in between. Based on past experience, one might expect that the epc17-1 functional, which provides the most delocalized densitiy, would yield the most accurate frequency for the PTM. However, this is not the case within the CNEO framework, where vibrational frequencies are obtained from the effective energy surface of CNEO rather than directly through the extent of proton densitiy delocalization. Although delocalization impacts the absolute zero-point energies, the accuracy of vibrational frequencies depends more on the relative energies, or more rigorously, the second-order derivatives of the energy surfaces. Therefore, although CNEO-DFT with epc17-1 produces a more delocalized density close to grid-based references while conventional DFT gives the most localized density, their performances in predicting vibrational frequencies can be equally bad. In contrast, CNEO-DFT with no-epc and with epc17-2 could yield more accurate results despite their proton densities are still too localized compared to grid-based references.

Interestingly, similar observations had been made in the development of NEO-TDDFT for calculating proton vibrational excitations. As shown in Table S2.1.1 of Ref. 55, the vibrational excitation energies from NEO-TDDFT with no-epc and with the epc17-2 functional both match well with grid-based reference values, whereas those from the epc17-1 functional

are far less accurate. Therefore, in both NEO-TDDFT and CNEO, it can be concluded that better proton densities are neither sufficient nor necessary for obtaining accurate vibrational frequencies. The accurate descriptions of vibrational frequencies may be a delicate balance of electronic effects and quantum delocalization effects. The CNEO framework offers an efficient way of calculating vibrational frequencies with NQEs incorporated, and the no-epc variant is the most straightforward way with least computational cost and easiest to reach SCF convergence. Therefore, we recommend the use of no-epc for CNEO vibrational spectrum calculations, until a more accurate electron-proton correlation functional becomes available. An alternative approach to advance this field may involve developing CNEO wave function theories, such as CNEO many-body perturbation theory and CNEO coupled cluster theory. These methods could offer more balanced descriptions of vibrational frequencies and proton densities, as well as provide deeper insights into electron-proton correlation effects. The development of these theoretical methods will be pursued in the future.

V. CONCLUSIONS

In conclusion, our investigation of a series of shared proton systems highlights the significant impact of nuclear quantum effects on the frequencies of proton transfer modes. Conventional DFT, due to its inability to capture the quantum nature of protons, fails to accurately describe the hydrogen-related vibrational modes. For PTMs, the frequency discrepancies can be as large as several hundred wavenumbers compared to experimental values. In contrast, CNEO accurately describes the hydrogen-related vibrational modes, even without any electron-proton correlations. For [A·H^+·A] type clusters, multiple peaks are associated with proton transfer and the CNEO method effectively captures this feature. The calculated IR spectra are in general consistent with experimental IR spectra, whereas conventional DFT often struggles with both frequencies and intensities for the PTMs.

We also evaluated the performance of two widely used multicomponent electron-proton correlation functionals (epc17-1 and epc17-2) within the CNEO framework. The calculated vibrational frequencies are sensitive to the choice of the functionals. Notably, the epc17-1 functional yields inaccurate vibrational frequencies, similar to those from DFT calculations, suggesting that it should be avoided for calculating molecular vibrational frequencies within the CNEO framework. In contrast, incorporating the epc17-2 functional in CNEO-DFT

calculations results in frequencies comparable to those obtained at the no-epc level. Given the additional computational cost of including electron-proton correlation functionals, we currently recommend performing CNEO-DFT calculations at the no-epc level for molecular vibration problems.

SUPPLEMENTARY MATERIAL

See the supplementary material for the OH bond lengths for equilibrium conformations of shared-proton complexes and normal modes of MeOH$-$H$^+-$HOMe.

ACKNOWLEDGMENTS

Yuzhuo Yang and Xi Xu thank the funding support from the Beijing Natural Science Foundation (No. 2234088), the National Natural Science Foundation of China (No. 22303006), the start-up funding (No. 310432108) from Beijing Normal University at Zhuhai, and the support from the Interdisciplinary Intelligence SuperComputer Center of Beijing Normal University at Zhuhai. Yuzhe Zhang and Yang Yang thank the funding support from the National Science Foundation under Grant No.2238473. The authors thank Mark A. Johnson for providing experimental data.

DATA AVAILABILITY

The data that support the findings of this study are available from the corresponding author upon reasonable request.

REFERENCES

[1]D. Marx, ChemPhysChem **7**, 1848 (2006).

[2]M. E. Tuckerman, D. Marx, M. L. Klein, and M. Parrinello, Science **275**, 817 (1997).

[3]K. R. Asmis, N. L. Pivonka, G. Santambrogio, M. Brümmer, C. Kaposta, D. M. Neumark, and L. Wöste, Science **299**, 1375 (2003).

[4]J. M. Headrick, J. C. Bopp, and M. A. Johnson, J. Chem. Phys. **121**, 11523 (2004).

[5]J. M. Headrick, E. G. Diken, R. S. Walters, N. I. Hammer, R. A. Christie, J. Cui, E. M. Myshakin, M. A. Duncan, M. A. Johnson, and K. D. Jordan, Science **308**, 1765 (2005).

[6]E. G. Diken, J. M. Headrick, J. R. Roscioli, J. C. Bopp, M. A. Johnson, and A. B. McCoy, J. Phys. Chem. A **109**, 1487 (2005).

[7]L. R. McCunn, J. R. Roscioli, M. A. Johnson, and A. B. McCoy, J. Phys. Chem. B **112**, 321 (2008).

[8]M. Kaledin, A. L. Kaledin, J. M. Bowman, J. Ding, and K. D. Jordan, J. Phys. Chem. A **113**, 7671 (2009).

[9]N. Agmon, H. J. Bakker, R. K. Campen, R. H. Henchman, P. Pohl, S. Roke, M. Thämer, and A. Hassanali, Chem. Rev. **116**, 7642 (2016).

[10]F. Mouhat, S. Sorella, R. Vuilleumier, A. M. Saitta, and M. Casula, J. Chem. Theory Comput. **13**, 2400 (2017).

[11]C. A. Reed, Acc. Chem. Res. **46**, 2567 (2013).

[12]M. Ceriotti, W. Fang, P. G. Kusalik, R. H. McKenzie, A. Michaelides, M. A. Morales, and T. E. Markland, Chem. Rev. **116**, 7529 (2016).

[13]W. Fang, J. Chen, Y. Feng, X.-Z. Li, and A. Michaelides, Int. Rev. Phys. Chem. **38**, 35 (2019).

[14]J. Guo, X.-Z. Li, J. Peng, E.-G. Wang, and Y. Jiang, Prog. Surf. Sci. **92**, 203 (2017).

[15]L. Wang, S. D. Fried, S. G. Boxer, and T. E. Markland, Proc. Natl. Acad. Sci. **111**, 18454 (2014).

[16]H.-D. Meyer and G. A. Worth, Theor. Chem. Acc. **109**, 251 (2003).

[17]H.-D. Meyer, WIREs Comput. Mol. Sci. **2**, 351 (2012).

[18]S. Habershon, D. E. Manolopoulos, T. E. Markland, and T. F. Miller, Annu. Rev. Phys. Chem. **64**, 387 (2013).

[19]T. E. Markland and M. Ceriotti, Nat. Rev. Chem. **2**, 1 (2018).

[20]A. D. Bochevarov, E. F. Valeev, and C. D. Sherrill, Mol. Phys. **102**, 111 (2004).

[21]T. Ishimoto, M. Tachikawa, and U. Nagashima, Int. J. Quantum Chem. **109**, 2677 (2009).

[22]F. Pavošević, T. Culpitt, and S. Hammes-Schiffer, Chem. Rev. **120**, 4222 (2020).

[23]X. Xu and Y. Yang, J. Chem. Phys. **152**, 084107 (2020).

[24]X. Xu and Y. Yang, J. Chem. Phys. **154**, 244110 (2021).

[25]X. Xu and Y. Yang, J. Chem. Phys. **153**, 074106 (2020).

[26]X. Xu, Z. Chen, and Y. Yang, J. Am. Chem. Soc. **144**, 4039 (2022).

[27]Z. Chen and Y. Yang, J. Phys. Chem. Lett. , 279 (2023).

[28]Y. Zhang, X. Xu, N. Yang, Z. Chen, and Y. Yang, J. Chem. Phys. **158**, 231101 (2023).

[29]X. Xu, J. Phys. Chem. A **127**, 6329 (2023).

[30]Y. Zhang, Y. Wang, X. Xu, Z. Chen, and Y. Yang, J. Chem. Theory Comput. **19**, 9358 (2023).

[31]Y. Wang, Z. Chen, and Y. Yang, J. Phys. Chem. A **127**, 5491 (2023).

[32]X. Zhao, Z. Chen, and Y. Yang, Chem. Phys. Rev. **5**, 041401 (2024).

[33]J. Langford, Y. Zhang, Z. Chen, and Y. Yang, J. Chem. Phys. **161**, 134302 (2024).

[34]Z. Chen, J. Zheng, D. Truhlar, and Y. Yang, Constrained Nuclear-Electronic Orbital Transition State Theory Using Energy Surfaces with Nuclear Quantum Effects (2024).

[35]Y. Yang, K. R. Brorsen, T. Culpitt, M. V. Pak, and S. Hammes-Schiffer, J. Chem. Phys. **147**, 114113 (2017).

[36]K. R. Brorsen, Y. Yang, and S. Hammes-Schiffer, J. Phys. Chem. Lett. **8**, 3488 (2017).

[37]K. R. Brorsen, P. E. Schneider, and S. Hammes-Schiffer, J. Chem. Phys. **149**, 044110 (2018).

[38]Z. Tao, Y. Yang, and S. Hammes-Schiffer, J. Chem. Phys. **151**, 124102 (2019).

[39]J. F. Capitani, R. F. Nalewajski, and R. G. Parr, J. Chem. Phys. **76**, 568 (1982).

[40]C. Lee, W. Yang, and R. G. Parr, Phys. Rev. B **37**, 785 (1988).

[41]Q. Sun, T. C. Berkelbach, N. S. Blunt, G. H. Booth, S. Guo, Z. Li, J. Liu, J. D. McClain, E. R. Sayfutyarova, S. Sharma, S. Wouters, and G. K.-L. Chan, WIREs Comput Mol Sci **8**, e1340 (2018).

[42]Q. Sun, X. Zhang, S. Banerjee, P. Bao, M. Barbry, N. S. Blunt, N. A. Bogdanov, G. H. Booth, J. Chen, Z.-H. Cui, J. J. Eriksen, Y. Gao, S. Guo, J. Hermann, M. R. Hermes, K. Koh, P. Koval, S. Lehtola, Z. Li, J. Liu, N. Mardirossian, J. D. McClain, M. Motta, B. Mussard, H. Q. Pham, A. Pulkin, W. Purwanto, P. J. Robinson, E. Ronca, E. R. Sayfutyarova, M. Scheurer, H. F. Schurkus, J. E. T. Smith, C. Sun, S.-N. Sun, S. Upadhyay, L. K. Wagner, X. Wang, A. White, J. D. Whitfield, M. J. Williamson, S. Wouters, J. Yang, J. M. Yu, T. Zhu, T. C. Berkelbach, S. Sharma, A. Y. Sokolov, and G. K.-L. Chan, J. Chem. Phys. **153**, 024109 (2020).

[43]A. H. Larsen, J. J. Mortensen, J. Blomqvist, I. E. Castelli, R. Christensen, M. Du\lak, J. Friis, M. N. Groves, B. Hammer, C. Hargus, E. D. Hermes, P. C. Jennings, P. B. Jensen, J. Kermode, J. R. Kitchin, E. L. Kolsbjerg, J. Kubal, K. Kaasbjerg, S. Lysgaard, J. B.

Maronsson, T. Maxson, T. Olsen, L. Pastewka, A. Peterson, C. Rostgaard, J. Schiøtz, O. Schütt, M. Strange, K. S. Thygesen, T. Vegge, L. Vilhelmsen, M. Walter, Z. Zeng, and K. W. Jacobsen, J. Phys.: Condens. Matter **29**, 273002 (2017).

[44]A. D. Becke, Phys. Rev. A **38**, 3098 (1988).

[45]C. Adamo and V. Barone, J. Chem. Phys. **110**, 6158 (1999).

[46]J.-D. Chai and M. Head-Gordon, J. Chem. Phys. **128**, 084106 (2008).

[47]K. Raghavachari, G. W. Trucks, J. A. Pople, and M. Head-Gordon, Chem. Phys. Lett. **157**, 479 (1989).

[48]T. H. Dunning, J. Chem. Phys. **90**, 1007 (1989).

[49]S. Grimme, A. Hansen, J. G. Brandenburg, and C. Bannwarth, Chem. Rev. **116**, 5105 (2016).

[50]S. Grimme, S. Ehrlich, and L. Goerigk, J. Comput. Chem. **32**, 1456 (2011).

[51]A. Najibi and L. Goerigk, J. Chem. Theory Comput. **14**, 5725 (2018).

[52]A. D. Boese, ChemPhysChem **16**, 978 (2015).

[53]Q. Yu, F. Pavošević, and S. Hammes-Schiffer, J. Chem. Phys. **152**, 244123 (2020).

[54]J. R. Roscioli, L. R. McCunn, and M. A. Johnson, Science **316**, 249 (2007).

[55]Y. Yang, T. Culpitt, and S. Hammes-Schiffer, J. Phys. Chem. Lett. **9**, 1765 (2018).

[56]T. Culpitt, Y. Yang, F. Pavošević, Z. Tao, and S. Hammes-Schiffer, J. Chem. Phys. **150**, 201101 (2019).